

Scalable kernel balancing weights in a nationwide observational study of hospital profit status and heart attack outcomes*

Kwangho Kim[†] Bijan A. Niknam[‡] José R. Zubizarreta[§]

Abstract

Weighting is a general and often-used method for statistical adjustment. Weighting has two objectives: first, to balance covariate distributions, and second, to ensure that the weights have minimal dispersion and thus produce a more stable estimator. A recent, increasingly common approach directly optimizes the weights toward these two objectives. However, this approach has not yet been feasible in large-scale datasets when investigators wish to flexibly balance general basis functions in an extended feature space. For example, many balancing approaches cannot scale to national-level health services research studies. To address this practical problem, we describe a scalable and flexible approach to weighting that integrates a basis expansion in a reproducing kernel Hilbert space with state-of-the-art convex optimization techniques. Specifically, we use the rank-restricted Nyström method to efficiently compute a kernel basis for balancing in nearly linear time and space, and then use the specialized first-order alternating direction method of multipliers to rapidly find the optimal weights. In an extensive simulation study, we provide new insights into the performance of weighting estimators in large datasets, showing that the proposed approach substantially outperforms others in terms of accuracy and speed. Finally, we use this weighting approach to conduct a national study of the relationship between hospital profit status and heart attack outcomes in a comprehensive dataset of 1.27 million patients. We find that for-profit hospitals use interventional cardiology to treat heart attacks at similar rates as other hospitals, but have higher mortality and readmission rates.

Keywords: Causal Inference; Observational Studies; Weighting; Convex Optimization; Propensity Score

*This work was supported through a grant from the Alfred P. Sloan Foundation (G-2020-13946) and an award from the Patient Centered Outcomes Research Initiative (PCORI, ME-2022C1- 25648). The authors report there are no competing interests to declare. This work was completed while Kwangho Kim was a research associate at Harvard Medical School.

[†]Department of Statistics, Korea University, 145 Anam-ro, Seongbuk-gu, Seoul, 02841, South Korea; email: kwanghk@korea.ac.kr.

[‡]Department of Biostatistics, Johns Hopkins Bloomberg School of Public Health, 615 N Wolfe St, Baltimore, MD 21205, United States; email: bniknam1@jh.edu.

[§]Departments of Health Care Policy, Biostatistics, and Statistics, Harvard University, 180 Longwood Avenue, Office 307-D, Boston, MA 02115, United States; email: zubizarreta@hcp.med.harvard.edu.

1 Introduction

1.1 Hospital profit status and heart attack care

For-profit organizations, including hospitals, are widespread across the US healthcare system. The impact of profit motive on treatment and outcomes is a major focus of healthcare research. For-profit status may possibly incentivize hospitals to provide more efficient care, leading to better patient outcomes. For-profit hospitals may also invest more in technology and human capital to improve competitiveness and potentially patient outcomes. Alternatively, higher reimbursement for interventional treatment may possibly incentivize them to use invasive treatments more frequently than medically necessary. For example, Medicare pays hospitals more for heart attack patients who receive percutaneous coronary intervention (PCI), a treatment that is essential in some cases but of ambiguous benefit in others, potentially incentivizing unnecessary use. Previous studies of subgroups of hospitals reached conflicting conclusions on both PCI treatment rates and patient outcomes (Sloan et al. 2003; Shah et al. 2007), emphasizing the need for a representative study of a comprehensive national sample.

1.2 Weighting for covariate adjustment in large-scale datasets

Covariate adjustment is essential in observational studies to remove bias due to differences in observed confounders. One method for adjustment is weighting, which uses each unit's probability of treatment assignment to form weighted samples that are free from differences due to observed confounders (Austin and Stuart 2015). Weighting attempts to remove bias by balancing observed covariate distributions while also producing robust and stable estimators. An appealing property of weighting is that it does not require explicit modeling of the outcome, and hence is part of the design stage of the study (Rubin 2006). Further, a single set of weights can in principle be used to examine multiple outcomes (Little and Rubin 2019).

Procedurally, there are two broad approaches to weighting (Ben-Michael et al. 2021). The modeling approach emphasizes the fit of a model for the probability of treatment assignment given observed covariates, or propensity score (Rosenbaum and Rubin 1983). However, covariate balance may be inadequate due to model misspecification or small samples; moreover, the weights may be highly variable and produce unstable estimators (Kang and Schafer 2007; Zubizarreta 2015). To address these challenges, the balancing approach attempts to balance covariates directly, often by solving a convex optimization problem to find the weights of minimum dispersion that balance functions of the covariates (see, e.g., Hainmueller 2012, Zubizarreta 2015). This affords control over the form and degree of balance while also targeting estimator stability. Thus, the balancing approach can have better finite-sample performance (Chattopadhyay et al. 2020).

Despite these appealing properties, the computational cost of many weighting algorithms prevents their scaling to the massive dimensions of many modern data sources in health sciences, which can reach millions of observations and hundreds of covariates. Moreover, to improve estimation accuracy, researchers increasingly recognize the importance of balancing richer covariate function classes beyond simple means and other low-dimensional parametric summaries. However, this additional complexity makes execution of weighting methods at scale even more challenging.

1.3 Contribution and outline

We propose a weighting approach that addresses practical barriers to the use of balancing methods in big data. Following Wong and Chan (2018) and Hazlett (2020), we adopt a kernel balancing approach which assumes the outcome regression functions are in a flexible function space represented by a kernel. Further, we use the recently developed rank-restricted Nyström approximation (Wang et al. 2019) that gives a provable approximate solution to the efficient kernel basis calculation problem. This allows us to construct the kernel basis functions in near-linear time and space, with strong relative-error guarantees. We then incor-

porate these functions into a quadratic program with linear constraints, which are efficiently solved via a specialized first-order alternating direction method of multipliers (Stellato et al. 2020), yielding the stable kernel balancing weights of minimum dispersion that approximately balance the covariate functions (Zubizarreta 2015). We analyze the worst-case bias bound of the resulting linear estimator and discuss its implications for parameter selection. We benchmark the proposed weighting estimator’s performance against common alternatives in extensive simulation studies, providing new insights into how weighting estimators perform at scale, finding that the proposed approach considerably outperforms others in terms of both accuracy and speed. Finally, we use the new approach in a national study of heart attack treatment and outcomes by hospital profit status.

The paper outline is as follows. Section 2 describes the setup, the balancing approach to weighting, and kernel balancing. Section 3 details the rank-restricted Nyström approximation, the operator splitting solver for quadratic programs, and the proposed scalable kernel balancing approach integrating the two concepts, along with an analysis of the worst-case bias bound for the resulting weighting estimator. Section 4 outlines the simulation study settings, examines the performance of the proposed estimator, and provides general insights into the speed and accuracy of various weighting estimators. Section 5 examines the relationship between hospital profit status and heart attack treatment and outcomes in a national Medicare dataset. Section 6 concludes.

2 Estimation framework

2.1 Two approaches to weighting

Consider an observational study with n triplets $(X, A, Y) \stackrel{iid}{\sim} \mathbb{P}$, where $X \in \mathcal{X} \subset \mathbb{R}^d$ is a vector of observed covariates, A is a binary treatment assignment indicator with the number of treated units $n_t = \sum_{i=1}^n A_i$ and control units $n_c = n - n_t$, and $Y \in \mathbb{R}$ is a real-valued outcome. Under the potential outcomes framework for causal inference (Rubin 1974), we

write $Y_i = A_i Y_i^1 + (1 - A_i) Y_i^0$, where Y_i^a is the potential outcome for unit i under treatment $A = a$; $a = 0, 1$. In our case study, $A = 1$ if a patient was admitted to a for-profit hospital, and $A = 0$ otherwise. Here, we wish to estimate the *average treatment effect on the treated* (ATT)¹,

$$\mathbb{E}(Y^1 - Y^0 \mid A = 1). \quad (1)$$

In order to identify the ATT from observational data, we invoke the following assumptions (Rosenbaum and Rubin 1983):

ASSUMPTION 2.1: (i) *Consistency*, $Y = Y^a$ if $A = a$; (ii) *Exchangeability*, $A \perp\!\!\!\perp Y^0 \mid X$; (iii) *Positivity*, $\mathbb{P}(A = 0 \mid X = x) > 0$ a.s. $[\mathbb{P}]$.

Given these assumptions, the ATT in (1) is identified by

$$\mathbb{E}(Y \mid A = 1) - \mathbb{E}\{\mathbb{E}(Y \mid X, A = 0) \mid A = 1\} \equiv \mathbb{E}(Y \mid A = 1) - \psi.$$

The first term can be estimated easily by taking a sample average. However, estimating ψ , the mean conditional potential outcomes of the treated under control, requires not only the aforementioned assumptions but also careful covariate adjustment.

A simple yet general weighting estimator for ψ is given by

$$\hat{\psi} = \sum_{\{i|A=0\}} \hat{w}_i Y_i \quad \text{for } \hat{w} \geq 0. \quad (2)$$

where $\hat{w} = (\hat{w}_1, \dots, \hat{w}_{n_c}) \in \mathbb{R}^{n_c}$ is the set of estimated weights that removes imbalances in covariate distributions such that after weighting adjustment, the control sample resembles the treated sample in aggregate.

In the modeling approach to weighting, we explicitly model the unknown propensity score

¹While we focus on estimating the ATT, our discussion also applies to the *average treatment effect* (ATE), and more generally to the *target average treatment effect* (TATE), $\mathbb{E}_{\mathbb{T}}(Y^1 - Y^0)$, where \mathbb{T} represents the measure of the target population of interest (Kern et al. 2016). The ATE and ATT are special cases of the TATE where $\mathbb{T} = \mathbb{P}$ and $\mathbb{T} = \mathbb{P}(A = 1)$, respectively.

$\pi(X) = \mathbb{P}(A = 1 \mid X)$, and then construct the weights \hat{w} using the estimated $\hat{\pi}$. One of the most widely-used modeling-based weighting estimators is the *Hajek estimator* defined by

$$\hat{\psi}_{\text{mod}} = \frac{1}{n} \sum_{i=1}^n \left\{ \frac{\hat{\pi}(X_i)(1 - A_i)}{1 - \hat{\pi}(X_i)} Y_i \right\} \bigg/ \frac{1}{n} \sum_{i=1}^n \left\{ \frac{\hat{\pi}(X_i)(1 - A_i)}{1 - \hat{\pi}(X_i)} \right\}. \quad (3)$$

The performance of model-based weighting estimators hinges upon the accuracy of estimation of $\hat{\pi}$. Often, flexible nonparametric models are employed for $\hat{\pi}$, but these approaches encounter difficulties when scaled to very large datasets (e.g., Zhou et al. 2017).

The balancing approach to weighting is a more recent alternative approach which avoids explicit modeling of π and rather directly optimizes for the weights. This approach can directly target not only covariate balance, but also the dispersion of the weights, thereby yielding a more stable estimator. Consequently, the balancing approach has been found to provide better finite-sample performance than the modeling approach (Chattopadhyay et al. 2020). Here, we focus on the stable balancing weights (SBW) (Zubizarreta 2015), which solve the following quadratic program

$$\begin{aligned} & \underset{w \in \mathbb{R}^{n_c}}{\text{minimize}} && \sum_{\{i|A=0\}} (w_i - \bar{w})^2 \\ & \text{subject to} && \left| \sum_{\{i|A=0\}} w_i B_b(X_i) - \frac{1}{n_t} \sum_{\{i|A=1\}} B_b(X_i) \right| \leq \delta, \quad b = 1, 2, \dots, M, \\ & && \sum_{\{i|A=0\}} w_i = 1, \quad w \geq 0, \end{aligned} \quad (4)$$

where $\bar{w} = \frac{1}{n_c} \sum_{\{i|A=0\}} w_i$, B_1, \dots, B_M are M real-valued basis functions of the covariates that span the model space in which the unknown outcome regression function is assumed to lie, and δ is a prespecified tolerance level for the maximum acceptable imbalance. We use $\hat{\psi}_{\text{bal}}$ to denote the weighting estimator when the set of weights \hat{w} represents the solution of (4). We focus on the stable balancing weights for two reasons. First, the objective function targets

the variance of the weights and hence (4) is a convex quadratic program (QP) to which we may apply a state-of-the-art algorithm to improve scalability. Second, the optimal weights have minimum variance and balance the covariates, thereby controlling the bias and variance of the resulting estimator, and achieving the semiparametric efficiency bound under certain regularity conditions (Wang and Zubizarreta 2020). Further, approximate rather than exact balancing makes the approach’s performance less sensitive to settings with limited covariate overlap. The parameter δ controls the trade-offs between covariate balance and the variance of the weights, and therefore the bias-variance trade-off of the resulting estimator. A smaller value of δ reduces imbalances and therefore bias due to differences in observed covariates, while a larger δ produces a set of weights with smaller variance and therefore a more stable estimator. In practice, subject-matter experts are typically consulted to ensure the choice of δ is suitable for the application at hand. However, some recent work has explored how to choose δ in an empirical fashion. For example, appealing to asymptotic theory, Hirshberg and Wager (2020) and Hirshberg et al. (2021) recommend selecting δ in the context of the dual formulation of the weighting problem and setting it to be roughly equivalent to the conditional variance of the outcome. Other automatic selection approaches have also been suggested (Kallus 2020; Wang and Zubizarreta 2020; Zhao 2019); however, more theoretical and empirical work remains to fully characterize their performance.

2.2 Kernel balancing

Let $\mu_0(X) = \mathbb{E}(Y^0 | X)$ be the outcome regression function in some model space \mathcal{M} . It can be shown that the bias of the weighting estimator (2) with the weights \hat{w} such that

$$\max_{\mu_0 \in \mathcal{M}} \left| \sum_{\{i|A=0\}} \hat{w}_i \mu_0(X_i) - \frac{1}{n_t} \sum_{\{i|A=1\}} \mu_0(X_i) \right| \leq \delta \quad (5)$$

is on the order of δ (Ben-Michael et al. 2021). Hence, to maximize the chance that the weighting adjustment eliminates the covariate imbalance in μ_0 , it is desirable to choose a flexible set of basis functions $\{B_1, \dots, B_M\}$ that spans a general model space for μ_0 . One such

space is the Reproducing Kernel Hilbert Space (RKHS). For a Mercer kernel $K : \mathcal{X} \times \mathcal{X} \rightarrow \mathbb{R}$ and a given sample of size n , the RKHS \mathcal{H}_K is defined by the completion of the function space

$$\left\{ f : f(x) = \sum_{i=1}^n \alpha_i K(X_i, x), \alpha_i \in \mathbb{R} \right\}$$

with respect to the norm $\|f\|_{\mathcal{H}_K} = \sqrt{\sum_{i=1}^n \sum_{j=1}^n \alpha_i \alpha_j K(X_i, X_j)} = \sqrt{\alpha^\top \mathbf{K} \alpha}$, $\forall f \in \mathcal{H}_K$, where $\alpha = (\alpha_1, \dots, \alpha_n)^\top \in \mathbb{R}^n$ and \mathbf{K} is the $n \times n$ kernel matrix in our observational data with $\mathbf{K}_{ij} = K(X_i, X_j)$. For a clearer conceptualization of the function space \mathcal{H}_K , define a feature map $\Phi(x) : x \mapsto [\sqrt{\lambda_1} \varphi_1(x), \sqrt{\lambda_2} \varphi_2(x), \dots]$, where $\{\lambda_j\}$ and $\{\varphi_j\}$ are, respectively, the eigenvalues and orthonormal eigenfunctions of the kernel operator such that $\int K(x, y) \varphi_j(y) dy = \lambda_j \varphi_j(x)$. Then by Mercer's Theorem it can be shown that $\Phi(x)^\top \Phi(y) = K(x, y)$, and that for any $f \in \mathcal{H}_K$, f can be expanded either in terms of K or in terms of the bases $\{\varphi_j(\cdot)\}_{j=1}^\infty$, such that

$$f(x) = \sum_{i=1}^n \alpha_i K(X_i, x) = \sum_{j=1}^\infty \beta_j \varphi_j(x) \quad (6)$$

for some $\alpha_i, \beta_j \in \mathbb{R}$. In the kernel balancing approach, we assume that $\mu_0 \in \mathcal{H}_K$ as follows.

ASSUMPTION 2.2: $\mathcal{M} = \mathcal{H}_K$ for a Mercer kernel K and its induced RKHS \mathcal{H}_K .

Letting the balancing constraints in (4) be $B_b(\cdot) = \varphi_b(\cdot)$, $b = 1, \dots, \infty$, we pursue approximate mean balance on the basis set for \mathcal{H}_K , $\{\varphi_j(\cdot)\}_{j=1}^\infty$, to control bias according to (5). By (6), this is equivalent to using $B_b(\cdot) = \mathbf{K}_b^\top$, $b = 1, \dots, n$, where \mathbf{K}_i denotes the i -th row of \mathbf{K} . In other words, one may use the n columns of \mathbf{K} as bases for μ_0 rather than $\{\varphi_j(\cdot)\}_{j=1}^\infty$. Note that \mathbf{K} can be constructed without computing φ_b . Achieving mean balance on columns of \mathbf{K} can also guarantee covariate balance in $\hat{\mu}_0$. If we find $\hat{\mu}_0$ as the solution to

the regularized problem

$$\min_{\mu_0 \in \mathcal{H}_K} \sum_{i=1}^n \mathcal{L}(\mu_0(X_i), Y_i^0) + \tau \Omega(\|\mu_0\|_{\mathcal{H}_K}), \quad (7)$$

for some loss function $\mathcal{L} : \mathbb{R}^2 \rightarrow \mathbb{R}$, monotone increasing function Ω , and $\tau > 0$, then by the representer theorem (Wahba 1990), $\hat{\mu}_0$ always has the form $\hat{\mu}_0(x) = \sum_{i=1}^n \alpha_i^* K(X_i, x) = \sum_{j=1}^{\infty} \beta_j^* \varphi_j(x)$ for some $\alpha_i^*, \beta_j^* \in \mathbb{R}$. Hence, the same argument applies as above.

However, incorporating n balancing constraints into the optimization is challenging for large n . Admitting the spectral decomposition, one may write $\mathbf{K} = U\Lambda U^\top$ where Λ is the diagonal matrix with a set of eigenvalues in decreasing order. Then under Assumption (2.2), the bias of the linear estimator (2) due to imbalance on \mathbf{K} is given by

$$\text{Bias}(\hat{\psi}; \mathbf{K}) := C_0 \left(\hat{w}^\top U_c - \frac{1}{n_t} \mathbf{1}_{n_t}^\top U_t \right) \Lambda U^\top \alpha_0, \quad (8)$$

for some $C_0 > 0$ and α_0 such that $\|\mu_0\|_{\mathcal{H}_K} = \sqrt{\alpha_0^\top \mathbf{K} \alpha_0}$, where U_c (U_t) are rows of U corresponding to the control (treated) units and $\mathbf{1}_{n_t}$ is the vector of ones of length n_t . Based on this finding, Hazlett (2020) proposed balancing the first $r \ll n$ eigenvectors of \mathbf{K} , i.e., the first r columns of U , rather than balancing all n columns of \mathbf{K} . While easier than balancing all n columns, this can still be prohibitive due to the high computational cost of the eigenvalue decomposition; standard algorithms for the eigenvalue decomposition of a dense $n \times n$ matrix require $O(n^2)$ -space and have $O(n^3)$ -time complexity. In the next section, we discuss an effective approximation method for \mathbf{K} and a scalable strategy for the corresponding basis function construction.

Remark 1 (Positivity under a model class). *Although positivity is not strictly required for identification under the assumption that $\mathcal{M} = \mathcal{H}_K$, it may play a role in estimation by influencing the feasibility of finding the weights in the balancing problem. At the extreme, one may not feasibly find weights if no control units have similar rows of \mathbf{K} as a given*

treated unit. However, the notion of positivity in this setting is more subtle than the standard positivity assumption, as there are several factors simultaneously affecting the feasibility of weighting solutions, including the type of kernel, bandwidth, tolerance level, and the observed sample at hand.

Remark 2 (Considerations for Kernel selection). *For a given a kernel K , the corresponding RKHS is unique. One desirable property for K is universal approximation, which allows us to approximate an arbitrary continuous function uniformly on the feature space induced by Φ (Micchelli et al. 2006). Following Hazlett (2020), we use the Gaussian kernel, which satisfies the universal approximation property. However, other kernels could also be considered depending on prior knowledge of the properties of the outcome regression function (see Micchelli et al., 2006, Section 3, for examples of universal kernels). When setting the kernel bandwidth, we likewise follow Hazlett (2020) by setting it to the column rank of X . Like the type of kernel, the chosen bandwidth may also affect both the performance and feasibility of the kernel balancing estimator. The optimal choices of the kernel and its bandwidth are important considerations in causal inference that warrant further investigation.*

3 Toward scalable and flexible weighting

3.1 Scalable kernel basis calculation using the rank-restricted Nyström approximation

The kernel approach provides a flexible way to balance functions of the covariates. However, its expensive computational cost presently prevents its use in large datasets. This problem can be surmounted with low-rank matrix approximations. Rather than compute the eigenvalue decomposition of the entire kernel, one may instead perform a partial singular value decomposition (SVD) (Lehoucq et al. 1998). However, the performance of this approach depends heavily on the singular spectrum structure of \mathbf{K} , and only realizes computational gains when \mathbf{K} is sparse. Another alternative is to use a class of randomized algorithms such

as the randomized QR decomposition or randomized SVD (Halko et al. 2011), but despite having good convergence, these algorithms still generally require $O(n^2)$ time.

A more general alternative is the Nyström method (e.g., Gittens and Mahoney 2016), an efficient technique for low-rank approximation of a full kernel matrix based on a subset of its columns. The method can substantially reduce the time complexity since only a portion of \mathbf{K} is sampled for computation. However, when n is extremely large, even a small matrix may no longer be small in practical terms, and the accuracy of the matrix approximation drastically declines if the number of sampled columns is too small. In this context, Pourkamali-Anaraki et al. (2018) note the limitations of traditional Nyström methods for very large data sets, a problem we address using a more recently introduced form of the Nyström method.

We adopt the rank-restricted Nyström method recently proposed by Wang et al. (2019). Unlike traditional Nyström methods, the rank-restricted method allows the target rank to be much smaller than the number of sampled columns while still providing guarantees on the relative-error bound. For $\mathbf{K} \in \mathbb{R}^{n \times n}$, we first sample a set of $m \ll n$ column indices \mathcal{I}_m (with the magnitude of sampled columns m also termed a *sketch size*). While various sampling or *sketching* schemes have been proposed (see, e.g., Kumar et al. 2012, and Table 1), we use uniform sampling here as its minimal computational cost per sampled column guarantees $O(n)$ time and hence has advantages for scalability. After sampling columns of \mathbf{K} , we form a matrix $C \in \mathbb{R}^{n \times c}$ with $C_{ij} = K(X_i, X_j)$, $i \in \{1, \dots, n\}$, $j \in \mathcal{I}_m$, and a matrix $W \in \mathbb{R}^{m \times m}$ with $W_{ij} = K(X_i, X_j)$, $i, j \in \mathcal{I}_m$. Then, the standard Nyström approximation for \mathbf{K} is

$$\widetilde{\mathbf{K}} = CW^+C^\top, \tag{9}$$

where W^+ is the Moore-Penrose (pseudo) inverse of W .

Because small singular values in W often result in numerical instability and thus large errors in W^+ , we mitigate this problem by adopting a commonly used regularization heuristic.

Table 1: Sufficient sketch sizes for popular sketching methods to construct the proposed Nyström approximation $(\tilde{\mathbf{K}})_s$ (Wang et al. 2019, Lemma 10). Here, $\epsilon \in (0, 1)$ and $\mu \in [1, \frac{n}{s}]$ denote the error parameter and the row coherence of V_s , respectively, where $V_s \Sigma_s V_s^\top$ is the truncated SVD of \mathbf{K}_s .

Sketching method	Sketch size (c)	Time complexity
Uniform sampling	$O\left(\frac{s\mu}{\epsilon} + s\mu \log s\right)$	$O(nc)$
Leverage sampling	$O\left(\frac{s}{\epsilon} + s \log s\right)$	$O(n^2 s)$
Gaussian projection	$O\left(\frac{s}{\epsilon}\right)$	$O(n^2 c)$
Subsampled randomized Hadamard transform	$O((s + \log n)(\epsilon^{-1} + \log s))$	$O(n^2 \log c)$
CountSketch	$O\left(\frac{s}{\epsilon} + s^2\right)$	$O(n^2)$

Specifically, for a *regularization parameter* $l < m$, we compute the SVD of W as $U_W \Lambda_W U_W^\top$ and let $W_l = U_{W,l} \Lambda_{W,l} U_{W,l}^\top$ be the truncated SVD of W , where $\text{diag}(\sigma_1, \dots, \sigma_l) = \Lambda_{W,l} \in \mathbb{R}^{l \times l}$.

Then, we use

$$\tilde{\mathbf{K}}_l = C W_l^{-1} C = C U_{W,l} \Lambda_{W,l}^{-1} U_{W,l}^\top C^\top \quad (10)$$

as a regularized version of $\tilde{\mathbf{K}}$.

Finally, we compute the rank-restricted Nyström approximation with a *target rank* s as

$$(\tilde{\mathbf{K}}_l)_s = D D^\top \quad \text{where} \quad D = C U_{W,l} \Lambda_{W,l}^{-1/2} \tilde{V}_{R,s} \equiv R \tilde{V}_{R,s} \in \mathbb{R}^{n \times s}, \quad (11)$$

where $\tilde{V}_{R,s}$ is the dominant s right singular vectors of $R = C U_{W,l} \Lambda_{W,l}^{-1/2}$, $s < l$.

Because the rank-restricted Nyström approximation offers an effective way to construct the s most relevant balancing constraints, the approach computes the weights faster while also yielding a more stable estimator. With uniform sampling, the time and space complexities to compute $(\tilde{\mathbf{K}}_l)_s$ are $O(m^3 + nml)$ and $O(nm + m^2)$, respectively. Since m , a proxy for our computational resources, increases at much slower rates than n in typical settings, both are now near-linear in n . Hence, (11) approximates the eigenvector-based kernel bases with major computing gains. This method is also much more computationally efficient in large

sample sizes than the rank- s randomized SVD, whose time complexity is $O(n^2s + s^3)$ (Li et al. 2014).

3.2 Scalable balancing weights using OSQP

Having described a practical way of computing the kernel representation, we next address optimization of the weights at scale. For large-scale convex optimization, the *alternating direction method of multipliers* (ADMM) is likely the most common solution method due to its computational efficiency (Boyd et al. 2011). However, ADMM has some limitations, such as its inability to detect infeasibility, the sensitivity of its performance to parameter selection and data setting, and its diminished speed advantage on high-accuracy settings. Recently, Stellato et al. (2020) developed the operator splitting solver for quadratic programs (OSQP), a state-of-the-art ADMM-based solver for general QPs that addresses these problems.

The OSQP algorithm is particularly well-suited to solving for the stable balancing weights in (4). First, the most time-intensive step of OSQP is solving the linear system of equations (Line 9 in Algorithm 1); however, since the coefficient matrix of the linear system is symmetric quasi-definite and sparse (with sparsity $\approx \frac{1}{n_c}$), a number of efficient algorithms can be applied to this step, such as the QDLDL factorization (Davis 2005). Second, the coefficient matrix of the linear system is always non-singular regardless of the step-size parameter values, preserving numerical stability without sacrificing speed. Finally, when careful tuning of δ is desired (for example, by using the bootstrap (Chattopadhyay et al. 2020; Wang and Zubizarreta 2020)), OSQP can execute this step much more efficiently through factorization caching and warm starting. See Appendix B for more details on ADMM and OSQP.

3.3 Implementation

This section describes an algorithm to formulate the proposed estimator incorporating kernel-based stable balancing weights. Assume we have obtained the rank- s Nyström approximation $(\widetilde{\mathbf{K}}_l)_s = DD^\top$ as in (11), and for the matrix D , let $D_t \in \mathbb{R}^{n_t \times s}$ and $D_c \in \mathbb{R}^{n_c \times s}$ be the rows

of D corresponding to the treated and control units, respectively. Given these inputs, the proposed kernel-based stable balancing weights are given by the optimal solution to the following quadratic program:

$$\begin{aligned} & \underset{\substack{w \in \mathbb{R}^{n_c} \\ z \in \mathbb{R}^{1+n_c+l}}}{\text{minimize}} && w^\top w - \frac{1}{n_c} w^\top \mathbb{1}_{n_c} \\ & \text{subject to} && Qw = z, z \in \mathcal{C}(\delta), \end{aligned} \tag{12}$$

for $Q = \begin{bmatrix} \mathbb{1}_{n_c} & \mathbb{0}_{n_c} & D_c \end{bmatrix}^\top$ and a set $\mathcal{C}(\delta) = \{z \mid l(\delta) \leq z \leq u(\delta)\}$ where

$$l(\delta) = \begin{bmatrix} 1 & \mathbb{0}_{n_c} & \overline{D}_t - \delta \end{bmatrix}^\top, \quad u(\delta) = \begin{bmatrix} 1 & \mathbb{1}_{n_c} & \overline{D}_t + \delta \end{bmatrix}^\top, \quad \delta = (\delta_1, \dots, \delta_s).$$

Here, $\mathbb{I}_r \in \mathbb{R}^{r \times r}$ is the $r \times r$ identity matrix, and $\mathbb{1}_r, \mathbb{0}_r \in \mathbb{R}^{1 \times r}$, the vectors of ones and zeros of length r , respectively; δ is a vector of maximum allowable imbalances specified by the investigator, and $\overline{D}_t \in \mathbb{R}^{1 \times s}$ is a row vector containing the mean of each column of D_t . Program (12) can be efficiently solved via OSQP. Algorithm 1 describes computation of the proposed estimator in detail. Note that the kernel balance constraints can also be used alongside traditional balance requirements for low-dimensional summaries of the covariates, such as their means.

Program (12) expresses the stable balancing weights problem (4) in the standard nomenclature of ADMM, with the approximated kernel basis D_{ib} as $B_b(X_i)$. Computation of D is informed by the scaling parameters m, l, s . The available computational capacity should be considered when selecting the sketch size m . Choices for the regularization parameter l and the target rank s are related to the relative-error bound analysis in the next section.

Algorithm 1: Fast stable kernel balancing weights

- 1 **input:** Sample Z_1, \dots, Z_n , vector δ , integers $s < l < m \ll n$, and kernel $K(\cdot, \cdot)$
 - 2 Sample a set \mathcal{I}_m of $m \ll n$ indices in $\{1, \dots, n\}$
 - 3 Form $C \in \mathbb{R}^{n \times m}$ with $C_{ij} = K(X_i, X_j)$, $i \in \{1, \dots, n\}$, $j \in \mathcal{I}_m$, and $W \in \mathbb{R}^{m \times m}$ with $W_{ij} = K(X_i, X_j)$, $i, j \in \mathcal{I}_m$
 - 4 Compute the rank- l truncated SVD of W as $W_l = U_{W,l} \Lambda_{W,l} U_{W,l}^\top$
 - 5 Compute the rank- s truncated SVD of $R = CU_{W,l} \Lambda_{W,l}^{-1/2}$ as $\tilde{U}_{R,s} \tilde{\Lambda}_{R,s} \tilde{V}_{R,s}^\top$, then compute $D = R \tilde{V}_{R,s}$
 - 6 Compute $Q, l(\delta), u(\delta)$ using (12)
 - 7 Choose parameters $\rho > 0$, $\sigma > 0$, and $\alpha \in (0, 2)$; initialize w^0, y^0, z^0 , and ν^0 ; and set $k = 0$
 - 8 **repeat**
 - 9 $(\tilde{w}^{k+1}, \nu^{k+1}) \leftarrow \text{solve } \begin{bmatrix} -(1+\sigma)\mathbb{1}_{n_c} & -Q^\top \\ -Q & \rho^{-1}\mathbb{1}_{1+n_c+s} \end{bmatrix} \begin{bmatrix} \tilde{w}^{k+1} \\ \nu^{k+1} \end{bmatrix} = - \begin{bmatrix} \sigma w^k - 1/n_c \mathbb{1}_{n_c} \\ z^k - \rho^{-1} y^k \end{bmatrix}$
 - 10 $\tilde{z}^{k+1} \leftarrow z^k + \rho^{-1}(\nu^{k+1} - y^k)$
 - 11 $w^{k+1} \leftarrow \alpha \tilde{w}^{k+1} + (1 - \alpha) w^k$
 - 12 $z^{k+1} \leftarrow \Pi_{C(\delta)}(\alpha \tilde{z}^{k+1} + (1 - \alpha) z^k + \rho^{-1} y^k)$
 - 13 $y^{k+1} \leftarrow y^k + \rho(\alpha \tilde{z}^{k+1} + (1 - \alpha) z^k - z^{k+1})$
 - 14 $w \leftarrow w_k, k \leftarrow k + 1$
 - 15 **until** *termination criterion satisfied*;
 - 16 **output:** $\sum_{i=1}^{n_c} w_i Y_{c,i}$, where Y_c is an outcome vector for the control units
-

3.4 Analysis of the worst-case bias bound

In the next theorem, we analyze a worst-case bound on the bias, $\text{Bias}(\hat{\psi}; \mathbf{K})$, in (8):

$$\sup_{\alpha} \left| \left(\hat{w}^\top U_c - \frac{1}{n_t} \mathbb{1}_{n_t}^\top U_t \right) \Lambda U^\top \alpha \right|,$$

where \hat{w} is the proposed kernel-based estimator obtained via (12).

Theorem 3.1. *Suppose that Assumptions (2.1) and (2.2) hold. Further assume that $\|\tilde{\mathbf{K}} - \tilde{\mathbf{K}}_l\|_2 \leq \frac{\sigma_l - \sigma_{l+1}}{2}$ and $\sup \|\alpha\|_2 < \infty$. Let $\epsilon \in (0, 1)$ be an error parameter, and W_l and \mathbf{K}_s be the best low-rank approximations for W^+ and \mathbf{K} with ranks l and s , respectively. Then, for*

all the column sampling schemes in Table 1, with high probability at least 0.9,

$$\begin{aligned} \sup_{\alpha} \left| \left(\hat{w}^\top U_c - \frac{1}{n_t} \mathbb{1}_{n_t}^\top U_t \right) \Lambda U^\top \alpha \right| &= (1 + \epsilon) \|\mathbf{K} - \mathbf{K}_s\|_* \\ &+ O\left(\|W^+ - W_l^{-1}\|_2 + \|W^+ - W_l^{-1}\|_F^2 + \delta\right), \end{aligned} \quad (13)$$

where \mathbf{K}_s is the best rank- s approximation of \mathbf{K} . $\|\cdot\|_2$, $\|\cdot\|_*$ and $\|\cdot\|_F$ are the 2-norm, the trace norm, and the Frobenius norm, respectively.

See Appendix A in Supplementary Materials for the formal definitions of the matrix norms and the proof. The above theorem provides an upper bound on the bias and dissects it into three components. The first component, $(1 + \epsilon) \|\mathbf{K} - \mathbf{K}_s\|_*$, pertains to the bias due to the degree of kernel matrix approximation. It provides guarantees on relative-error trace norm approximation of the rank- s Nyström approximation without regularization. While the magnitude of this bias component may be reduced by choosing a larger value for s , this decision must be informed by choices for the other scaling parameters l and m as well as our error tolerance (see Remark 3). The second component of the bias, $\|W^+ - W_l^{-1}\|_2 + \|W^+ - W_l^{-1}\|_F^2$, represents the additive error due to the regularization step described in (10), and declines to zero with no regularization. Typically, we expect the second component to be much smaller than the first. The third and final component is the bias from the residual covariate imbalance after weighting, which is directly controlled by the tolerance vector δ governing the balancing constraints.

Remark 3. *[Scaling parameter selection] The upper bound in (3.13) depends on sketching schemes, as well as the scaling parameters m, l, s , error parameter ϵ , and matrix coherence $\mu \in \left[1, \frac{n}{s}\right]$ of the dominant s -dimensional singular space of \mathbf{K} . Although it is often not straightforward to characterize this upper bound in real datasets, some guidelines for selecting scaling parameters could be established. In Table 1, we provide sufficient sketch sizes m in terms of s, ϵ, μ . While a larger s better approximates the original kernel matrix, it must be some fraction of m , and it is desirable to set m as small as possible since it is a proxy*

for available computational resources. Thus, balancing these two sources of error requires choosing an s value that is sufficiently large to reduce error from matrix approximation, while also being a sufficiently small fraction of m . It is known that when uniform sampling is used to form the Nystrom approximation $m = \tilde{O}\left(\frac{s\mu}{\epsilon}\right)$ (Wang et al. 2019, Lemma 10). Hence, if one sets $\log s \sim \frac{1}{\epsilon}$, then the chosen m should be on the order of $\frac{s\mu}{\epsilon}$. When the budget of column samples m must to be fixed, the target rank could be $s \sim \frac{m}{\mu/\epsilon}$ where m is at least $\mu/\epsilon > 1$ times larger than s . The coherence parameter μ can be estimated from the truncated SVD of \mathbf{K} (see, e.g., Mohri and Talwalkar 2011). The regularization parameter l should remain as close to m as possible as long as σ_l is not extremely small, guaranteeing numerical stability of $\Lambda_{W,l}^{-1}$. Unfortunately, there is no theory for the choice of l as it is related to the finite precision error. Following Wang et al. (2019), we apply a simple heuristic that $l = \lceil \frac{s+m}{2} \rceil$. Future theoretical and empirical work is required for optimal scaling parameter selection, as well as characterizing how large the upper bound could be in real datasets.

4 Simulation study

We study the computational performance and estimation accuracy of several modeling and balancing weighting methods. We extend the simulation design by Hainmueller (2012) to encompass nonlinear treatment assignment processes and sample sizes up to a million.

4.1 Study design

Consider an observational study with continuous and binary covariates generated as follows

$$\begin{bmatrix} X_1 \\ X_2 \\ X_3 \end{bmatrix} \sim N\left(\begin{bmatrix} 0 \\ 0 \\ 0 \end{bmatrix}, \begin{bmatrix} 2 & 1 & -1 \\ 1 & 1 & -0.5 \\ -1 & -0.5 & 1 \end{bmatrix}\right), \quad X_4 \sim \text{Unif}[-3, 3], \quad X_5 \sim \chi_1^2, \quad X_6 \sim \text{Bern}[0.5].$$

Using these six covariates, we generate the outcome and treatment variables as

$$Y = (X_1 + X_2 + X_5)^2 + \eta, \quad \eta \sim N(0, 1), \quad (14)$$

$$A = \mathbb{1} \left\{ X_1^2 + 2X_2^2 - 2X_3^2 - (X_4 + 1)^3 - 0.5 \log(X_5 + 10) + X_6 - 1.5 + \varepsilon > 0 \right\}, \quad (15)$$

where $\varepsilon \sim N(0, \sigma_\varepsilon^2)$. We consider two settings with $\sigma_\varepsilon^2 = 30$ and $\sigma_\varepsilon^2 = 100$, hereafter referred to as the *weak overlap* and *strong overlap* settings, respectively. We define untransformed covariates $X = (X_1, X_2, X_3, X_4, X_5, X_6)$ and transformed covariates $X^* = (X_1 X_3, X_2^2, X_4, X_5, X_6)$. For each σ_ε^2 , we consider each interaction of treatment assignment mechanism and accuracy of covariate specification across five sample sizes: $n \in \{2 \cdot 10^3, 5 \cdot 10^3, 10^4, 10^5, 10^6\}$. In this design, the ATT equals zero by construction. To separate design from analysis and focus on scalability and speed, we based the weighting estimator (2) solely on $\hat{\pi}$; however, it can be augmented by an outcome model to form a doubly-robust estimator as in Robins and Rotnitzky (1995).

Estimation of the ATT by weighting requires explicit modeling of π for $\hat{\psi}_{\text{mod}}$ in the modeling approach, or solving the QP (12) to obtain $\hat{\psi}_{\text{bal}}$ in the balancing approach. We consider various methods, including some considered useful for large-scale modeling or optimization. For practicality, we focus on methods in readily available R packages. For consistent comparisons of balancing estimators, we fix $\delta = 0.0005$ across all methods. However, we also evaluate performance when selecting δ in a data-driven fashion using the algorithm in Chattopadhyay et al. (2020).

We consider nine methods for $\hat{\psi}_{\text{mod}}$ and seven methods for $\hat{\psi}_{\text{bal}}$, for a total of 16 methods classified into six groups (see Table 2. For $\hat{\psi}_{\text{mod}}$, Group M1 methods use logistic regression (or GLM) to model the propensity score. Group M2 contains lasso algorithms with the tuning parameter selected via 10-fold cross validation. In Groups M1 and M2, the regression models for π add quadratic terms and all pairwise products of observed covariates. Group M3 includes three common nonparametric algorithms: random forests, kernel ridge regression,

and generalized additive models using splines. For $\hat{\psi}_{\text{bal}}$, we solve (12) where we use the Gaussian kernel and set $m = 300$, $l = 200$, $s = 100$ for the Nyström approximation procedure. Group B1 includes open-source QP solvers in R. Group B2 studies two commercial solvers. Finally, Group B3 includes three state-of-the-art ADMM-based solvers aimed at reducing processing time and used with the kernel balancing approach. For OSQP, we use the same parameters as Stellato et al. (2020).

We assess estimator performance using the root-mean-squared error (RMSE) defined by $\left\{ \frac{1}{S} \sum_{j=1}^S (\hat{\psi}_j - \psi)^2 \right\}^{1/2}$ averaged across $S = 500$ simulations, and quantify the computational cost in average central processing unit (CPU) time across simulations, which we report in seconds unless otherwise noted. All simulations were completed using the Harvard Faculty of Arts and Sciences Research Computing clusters with available memory fixed at 128GB. In the results tables, we write ‘F’ when the optimization process failed in more than half the simulations, and ‘M’ when the system ran out of memory in more than half the simulations.

4.2 Empirical results

Table 3 shows estimation accuracy under weak overlap. The proposed kernel balancing estimators $\hat{\psi}_{\text{bal}}$ substantially outperform the modeling estimators $\hat{\psi}_{\text{mod}}$ at all considered sample sizes, especially in small to moderate ones, regardless of covariate specification; however, gaps between $\hat{\psi}_{\text{bal}}$ and $\hat{\psi}_{\text{mod}}$ are smaller with transformed covariates X^* . Performance varied greatly within the class of modeling approaches; in particular, random forests were most successful at larger sample sizes. We do not report results for kernel-based stable balancing weights without the Nyström approximation, since no methods were successful for samples of 100,000 or more.

Because the average CPU time did not appreciably vary across simulation settings, we present only their averages in Table 4. For $\hat{\psi}_{\text{bal}}$, forming the kernel basis requires less computation time than solving the QP, demonstrating the efficiency of the Nyström approximation in

Table 2: Description of modeling and solution methods used in the simulation study.

	Method	R package	Description
Modeling Approach	M1. Logistic regression	<code>glm</code>	Commonly used method to fit logistic regression models in R
		<code>sgdglm</code>	Stochastic gradient descent methods for estimation with big data (Tran et al. 2015)
	M2. Regularized regression	<code>glmnet</code>	Lasso via coordinate descent (Friedman et al. 2010)
		<code>biglasso</code>	Scalable lasso for big data (Zeng and Breheny 2017)
		<code>oem</code>	Lasso for tall (large n) data (Xiong et al. 2016)
		<code>penreg</code>	ADMM-based lasso implementation (Boyd et al. 2011) (<code>admm.lasso</code> in results)
	M3. Non-parametric regression	<code>ranger</code>	Fast implementation for Random Forests
		<code>DRR</code>	Fast implementation for Kernel Ridge Regression (<code>kernel.ridge</code> in results)
		<code>bam</code>	Generalized additive model using splines for big data (Wood et al. 2015)
	Balancing Approach	B1. Open-source solvers	<code>quadprog</code>
<code>qpoases</code>			QP solver based on parametric active-set algorithm (Ferreau et al. 2014)
B2. Commercial solvers		<code>gurobi</code>	Large scale commercial optimizer by <i>Gurobi Optimization</i>
		<code>Rmosek</code>	Large scale commercial optimizer by <i>Mosek ApS</i>
B3. ADMM-based solvers		<code>osqp</code>	Operator splitting solver for QP (OSQP) (Stellato et al. 2020)
		<code>pogs</code>	ADMM-based graph form solver (POGS) (Fougner and Boyd 2018)
		<code>scs</code>	Operator splitting conic solver (SCS) (O’donoghue et al. 2016)

the kernel balancing algorithm. When solving the same QP (12), OSQP was faster than the commercial solvers MOSEK and Gurobi, by about an order of magnitude in the case of the latter. The GLM and OSQP methods were fastest, taking only seconds to find the optimal weights even in the largest sample size of one million. In contrast, the lasso and non-

Table 3: Root-mean square error (RMSE) under weak overlap. Each cell contains the RMSE for each combination of method, sample size, and covariate specification, averaged across 500 simulations. “M” signifies the system ran out of memory in more than half the simulations, while “F” signifies that the optimization process failed to obtain a weighting solution in more than half the simulations.

		X correctly specified (X)					X transformed (X^*)				
		n									
Method		2k	5k	10k	100k	1M	2k	5k	10k	100k	1M
$\hat{\psi}_{\text{mod}}$	glm	1.72	1.29	1.20	1.19	1.18	1.85	1.37	1.30	1.18	1.18
	sgdglm	1.72	1.29	1.20	1.19	1.18	1.86	1.37	1.31	1.18	1.19
	glmnet	2.20	1.18	0.68	0.23	0.12	4.57	1.79	0.67	0.39	0.35
	biglasso	2.57	1.08	0.65	0.22	0.12	5.23	1.68	0.68	0.39	0.35
	oem	3.37	1.27	0.79	0.26	0.12	6.47	2.97	0.79	0.40	0.35
	admm.lasso	3.83	1.59	0.84	0.29	0.15	7.29	3.04	1.07	0.70	0.51
	ranger	0.71	0.33	0.22	0.15	0.09	0.97	0.41	0.36	0.27	0.22
	kernel.ridge	1.87	1.19	1.01	0.89	M	6.26	6.07	5.59	4.87	M
	bam	2.84	1.31	1.20	1.19	1.18	3.37	1.95	1.25	1.19	1.18
$\hat{\psi}_{\text{bal}}$	quadprog	0.31	0.20	0.15	F	F	0.51	0.34	0.33	F	F
	qpoases	0.32	0.22	0.15	F	F	0.65	0.34	0.24	F	F
	gurobi	0.19	0.13	0.09	0.04	0.02	0.31	0.19	0.15	0.08	0.05
	Rmosek	0.19	0.13	0.10	0.04	0.02	0.31	0.20	0.15	0.08	0.05
	osqp	0.19	0.03	0.10	0.04	0.02	0.31	0.19	0.16	0.08	0.05
	pogs	0.31	0.20	0.15	M	M	0.59	0.36	0.29	M	M
	scs	0.25	0.22	0.19	0.15	0.10	0.55	0.38	0.25	0.18	0.15

parametric methods required much more time at that sample size, in some cases hundreds of times more than GLM and OSQP. Although not presented here, the OSQP and GLM-based estimators took under a minute on average to handle a simulated dataset of 10 million observations, whereas the slowest methods took up to days.

Several methods faced difficulties at larger sample sizes, particularly $\hat{\psi}_{\text{bal}}$ approaches. At samples $\geq 100,000$, the open-source solvers failed to converge, while the system ran out of memory when attempting to execute POGS, perhaps because it cannot accommodate sparse matrices. Among $\hat{\psi}_{\text{mod}}$ approaches, kernel ridge regression ran out of memory at 1 million observations.

Results for RMSE, CPU time, convergence, and memory exhaustion in the strong covari-

Table 4: Average CPU time across simulation settings. Each cell contains the CPU time for each combination of method, sample size, and covariate specification, averaged across 500 simulations. All values are reported in seconds unless specified as being in hours (“hr”). “M” signifies the system ran out of memory in more than half the simulations, while “F” signifies that the optimization process failed to obtain a weighting solution in more than half the simulations.

		Time (in seconds unless otherwise noted)					
		n	2k	5k	10k	100k	1M
Method							
$\hat{\psi}_{\text{mod}}$	glm		<0.1	<0.1	<0.1	0.4	8.6
	sgdglm		<0.1	<0.1	<0.1	0.3	5.0
	glmnet		1.0	1.8	4.4	18	362
	biglasso		9.2	12	20	266	0.8hr
	oem		38	81	224	0.6hr	5hr
	admm.lasso		1.3	2.7	6.3	15	311
	ranger		8.7	30	128	0.4hr	3hr
	kernel.ridge		1.1	3.6	29	0.3hr	M
	bam		0.7	1.6	3.8	21	210
$\hat{\psi}_{\text{bal}}$	quadprog		0.9	15	119	F	F
	qpoases		48	127	392	F	F
	gurobi		<0.1	<0.1	0.5	6.3	94
	Rmosek		<0.1	<0.1	<0.1	4.2	37
	osqp		<0.1	<0.1	<0.1	3.2	9.6
	pogs		3.7	46	305	M	M
	scs		<0.1	5.3	14.5	27	169

ate overlap setting were generally consistent with those in weak overlap, but with smaller performance gaps between $\hat{\psi}_{\text{mod}}$ and $\hat{\psi}_{\text{bal}}$ (see Appendix C for details).

As noted in Section 3.2, the OSQP algorithm facilitates factorization caching and warm starting for even better computational efficiency when multiple iterations are required, such as for data-driven selection of δ . To demonstrate, we repeatedly solved a sequence of OSQP-based weighting problems in the same simulation settings using 100 different values of δ . The results showed that the OSQP algorithm achieved an additional 2.4-fold improvement in CPU time on average, whereas the commercial solvers did not exhibit such efficiency gains (see Appendix D).

5 A national study of heart attack care by hospital profit status

Heart attacks are generally treated with either interventional cardiology through percutaneous coronary intervention (PCI), or alternatively medical management. In the more severe subtype known as ST-elevation MIs, PCI is generally recommended. However, older patients are much more likely to have non-ST-elevation MIs, and guidelines are less clear on PCI use in this subtype and more generally among older patients with complex comorbid conditions (Lawton et al. 2022). Thus, clinical decision-making in this setting can be affected by both individual physician practice style and the norms of the institutions where they work. Medicare reimburses hospitals more when patients receive interventional cardiology, possibly incentivizing for-profit hospitals to do so more often. We asked whether for-profit hospitals were more likely to use interventional cardiology on heart attack patients than other hospitals, and whether patients outcomes differed. Two previous studies reported opposing results on relationships between profit status, PCI use, and outcomes. Sloan et al. (2003) found for-profit hospitals had higher rates of PCI than other hospitals yet similar mortality rates. In contrast, Shah et al. (2007) found similar rates of PCI use among non-ST elevation MI cases. However, these studies had fewer than 160,000 patients and used data from small numbers of hospitals in voluntary reporting systems; for example, Shah et al. (2007) studied only 58 for-profit hospitals.

To build on previous work by applying our proposed methods to a much larger and more representative sample, we studied a national dataset of Medicare administrative claims from the Centers for Medicare & Medicaid Services (CMS) for patients admitted to short-term acute-care hospitals for initial treatment of heart attack. We studied 1,273,636 Medicare beneficiaries hospitalized for heart attack between October 1, 2010 and November 30, 2019. We defined treatment as admission to a for-profit hospital, and control as admission to other types of hospitals.

A fair comparison of for-profit and control hospitals requires careful adjustment for differences in potentially confounding covariates. For example, heart attack treatment and outcomes can be affected by patient demographics and contemporary clinical guidelines. Thus, we adjusted for patient age on admission, sex, race, and admission year. The type of heart attack also strongly affects treatment and prognosis, as ST-elevation Myocardial Infarctions (STEMIs) are much more likely to receive PCI but are also much more severe than Non-ST-Elevation Myocardial Infarctions (NSTEMIs). Thus, we defined these by checking the inpatient record for corresponding International Classification of Diseases, 9th Revision, Clinical Modification (ICD-9-CM) or ICD-10-CM principal diagnosis codes. We then included covariates for these types of heart attack in the adjustment model. We also adjusted for emergent admission type and history of PCI or coronary artery bypass grafting (CABG) surgery. As comorbid risk factors such as history of diabetes, renal disease, or stroke can affect both prognosis and likelihood of receiving PCI, we also checked the inpatient records for evidence of a set of 43 comorbidities drawn from risk models maintained by CMS, concentrating on conditions noted as present on admission (POA). This screening only counted diagnoses explicitly documented as already existing upon the patient’s admission to the hospital rather than those noted as having occurred after the patient was admitted.

Patients may choose where to live in part on local healthcare resources, which can affect both selection into hospitals and the outcome. Thus, we also defined county-level measures of hospital characteristics such as academic affiliation, nurse staffing levels, size in number of beds, available cardiac technologies, and urban location, for a total of 17 hospital characteristics. This partially addresses selection bias due to residential choice based on potential medical need.

While the simulations included 6 adjustment covariates, our case study includes 70 patient covariates and 17 area-level hospital characteristics for a total of 87 covariates. Given the additional complexity arising from this much number of covariates and the size of the dataset

(over 1 million control patients and 1.27 million in total), we proceeded with the stable kernel balancing approach as it showed excellent computational efficiency without diminished estimator accuracy.

To make the assumption of conditional exchangeability more plausible in this demonstration of the method, we were careful to leverage the Medicare data as described above to adjust for as many observable pre-treatment covariates as possible such as demographics, heart attack type, risk factors, and hospital market characteristics. However, as this is an observational study, it is possible for there to be omitted unobserved confounders.

We used the proposed weighting methods to balance the 87 covariates and functions thereof, in order to estimate the average treatment effect on the treated; i.e., the effect of for-profit admission on the likelihood of receiving PCI. We assessed balance using target absolute standardized mean differences (TASMD) (Chattopadhyay et al. 2020), considering the for-profit and control groups balanced if no TASMD exceeded 0.1. Because the same set of weights can in principle be used to examine multiple endpoints, we used the weights to assess PCI use and several outcomes: mortality within 30 days of admission, length of stay, and readmission within 30 days of discharge.

5.1 Kernel balance

Table 5 shows selected characteristics of 206,948 patients from 775 for-profit and 1,066,780 patients from 2,763 control hospitals. See Appendix E for a balance table showing all 87 covariates.

Because heart attack is an acute condition, the time and place of its occurrence is not easily predictable and patients are usually brought to the closest hospital; hence, many characteristics such as age and several comorbidities are fairly well-balanced, although a number of imbalances persist and require adjustment. While the occurrence of heart attack in relation to the type of nearby hospital may be somewhat haphazard, the distribution of patient race as well as the characteristics of the hospitals in their counties are not. In

Table 5: Selected Covariates and Sample Size before Weighting. The table shows selected un-weighted covariate means and sample sizes among all patients admitted to for-profit hospitals or other hospitals, along with the target absolute standardized mean difference (TASMD) before weighting.

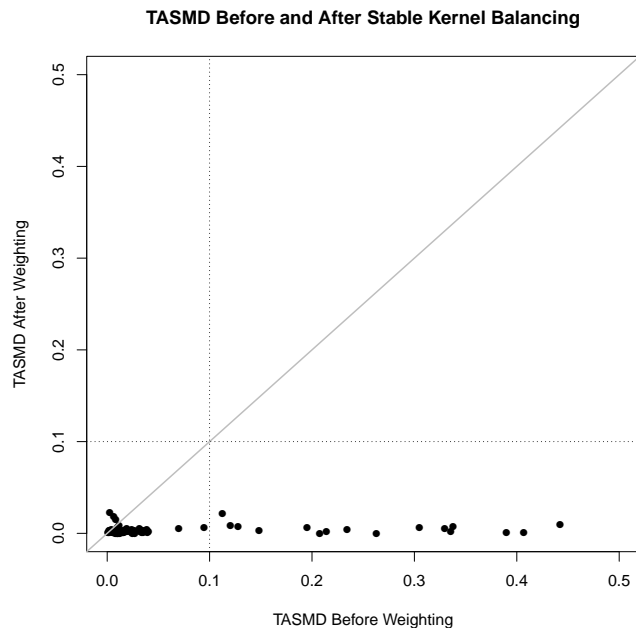
Covariate (% unless noted) / Sample Size	For-Profit	Controls	TASMD Before
<i>Demographic Characteristics</i>			
Age at admission (years, mean)	79.0	79.3	0.03
Female	47.8%	47.7%	0.00
Non-Hispanic White	79.0%	84.2%	0.13
Black	8.3%	7.8%	0.02
Hispanic	8.6%	4.4%	0.15
<i>Comorbidities Present on Admission</i>			
Diabetes	37.6%	37.1%	0.01
Heart Failure	43.5%	43.8%	0.01
Valvular Disease	15.6%	19.1%	0.09
<i>County of Residence Hospital Characteristics</i>			
Small Size (< 251 beds)	79.5%	72.9%	0.44
Nonteaching	87.6%	81.5%	0.41
<i>Sample Size</i>			
Patients	206,948	1,066,670	
Hospitals	775	2,763	

particular, patients admitted to for-profit hospitals were more likely to be nonwhite, and more likely to reside in counties where hospitals tended to be smaller and nonteaching. Given the policy importance of health equity, these community differences emphasize the need to benchmark for-profit hospital performance.

We used the same kernel and scaling parameters as in the simulations. However, to prioritize estimator accuracy in the case study, we used the high-accuracy setting with a much stricter termination criterion and solution polishing (Stellato et al. 2020, Section 4), and set $\delta = 0$ rather than $\delta = 0.0005$. These made the QP more difficult to solve, but favored estimator accuracy.

The stable kernel balancing algorithm efficiently produced excellent balance. Figure 1 shows that despite large initial imbalances, the weighting algorithm successfully balanced all covariates with all TASMDs after weighting well below 0.1, and none exceeding 0.03. In our

Figure 1: Each dot represents the Target Absolute Standardized Mean Difference (TASMD) of one of 87 covariates between for-profit and control hospitals before and after weighting.



dataset of 1.27 million patients, the kernel basis was computed in just 32.3 seconds, while the OSQP algorithm solved for the stable kernel balancing weights in 132 seconds.

5.2 Heart attack treatment and outcomes

Table 6 shows treatment and outcomes by hospital profit status after weighting. We found that for-profit hospitals used PCI at almost the same rate as control hospitals, which aligns with the more recent work by Shah et al. (2007), but conflicts with the earlier study by Sloan et al. (2003). Differences between our study and previous ones may also arise because we used a national sample of hospitals rather than sets of hospitals in voluntary reporting programs.

Despite similar PCI use, for-profit hospitals had significantly higher 30-day mortality relative to control hospitals, a finding that differs from the older study by Sloan et al. (2003). Compared to more contemporary work by Horwitz et al. (2017), we found a larger difference in mortality; however, their analysis pooled patients hospitalized for various reasons.

Table 6: PCI Use and Outcomes by Hospital Profit Status. The table shows outcome means among for-profit hospital patients, weighted outcome means among control hospital patients, and a 95% confidence interval for the difference.

Measure (percent unless noted)	For-Profit	Control	Difference	95% CI
Received PCI	33.2	33.1	0.1	(-0.1, 0.3)
30-day Mortality	14.3	13.9	0.4	(0.2, 0.6)
Length of Stay (days)	5.76	5.63	0.13	(0.10, 0.15)
30-day Readmission/IP Death	19.2	18.2	0.9	(0.7, 1.1)
30-day Readmission Only	11.5	10.6	0.8	(0.6, 0.9)

Length of stay was significantly but not meaningfully longer at for-profit hospitals. However, readmission rates were significantly and meaningfully higher at for-profit hospitals.

6 Summary

In this paper, we describe a weighting approach that overcomes previous barriers to the use of the balancing approach at large scales. We show that the rank-restricted Nyström approximation makes it computationally feasible to find a set of general functions of the covariates in an RKHS. We describe how the kernel basis from the Nyström approximation can be efficiently balanced via a modern ADMM-based convex optimization method. Our extensive simulation study shows that the proposed estimator has superior computation speed relative to other balancing approaches and even logistic regression-based modeling approaches. Moreover, this efficiency gain does not diminish the proposed estimator’s accuracy, as it performed as well as or better than other approaches in most simulation settings. Hence, our study provides new insights into the performance of weighting estimators in large datasets.

We used the proposed approach in a large observational study of heart attack treatment and outcomes in for-profit and control hospitals in a national Medicare dataset. We achieved excellent balance in under 3 minutes. After adjustment, for-profit hospitals used PCI at similar rates as others, but had significantly higher readmission rates. Future work could examine the impact of Medicare’s Hospital Readmissions Reduction Program on for-profit

hospitals.

7 Software

The proposed algorithm can be implemented in R with the code provided in <https://github.com/kwangho-joshua-kim/osqp-kernel-sbw>.

References

- Austin, P. C. and Stuart, E. A. (2015), “Moving towards best practice when using inverse probability of treatment weighting (IPTW) using the propensity score to estimate causal treatment effects in observational studies,” *Statistics in Medicine*, 34, 3661–3679.
- Ben-Michael, E., Feller, A., Hirshberg, D. A., and Zubizarreta, J. R. (2021), “The balancing act in causal inference,” *arXiv preprint arXiv:2110.14831*.
- Boyd, S., Parikh, N., and Chu, E. (2011), *Distributed optimization and statistical learning via the alternating direction method of multipliers*, Now Publishers, Inc.
- Chattopadhyay, A., Hase, C. H., and Zubizarreta, J. R. (2020), “Balancing vs modeling approaches to weighting in practice,” *Statistics in Medicine*, 39, 3227–3254.
- Davis, T. A. (2005), “Algorithm 849: A concise sparse Cholesky factorization package,” *ACM Transactions on Mathematical Software (TOMS)*, 31, 587–591.
- Ferreau, H. J., Kirches, C., Potschka, A., Bock, H. G., and Diehl, M. (2014), “qpOASES: A parametric active-set algorithm for quadratic programming,” *Mathematical Programming Computation*, 6, 327–363.
- Fougnier, C. and Boyd, S. (2018), “Parameter selection and preconditioning for a graph form solver,” in *Emerging Applications of Control and Systems Theory*, Springer, pp. 41–61.
- Friedman, J., Hastie, T., and Tibshirani, R. (2010), “Regularization paths for generalized linear models via coordinate descent,” *Journal of Statistical Software*, 33, 1–22.
- Gittens, A. and Mahoney, M. W. (2016), “Revisiting the Nyström method for improved large-scale machine learning,” *The Journal of Machine Learning Research*, 17, 3977–4041.
- Goldfarb, D. and Idnani, A. (1983), “A numerically stable dual method for solving strictly convex quadratic programs,” *Mathematical Programming*, 27, 1–33.

- Hainmueller, J. (2012), “Entropy balancing for causal effects: A multivariate reweighting method to produce balanced samples in observational studies,” *Political Analysis*, 20, 25–46.
- Halko, N., Martinsson, P.-G., and Tropp, J. A. (2011), “Finding structure with randomness: Probabilistic algorithms for constructing approximate matrix decompositions,” *SIAM review*, 53, 217–288.
- Hazlett, C. (2020), “KERNEL BALANCING,” *Statistica Sinica*, 30, 1155–1189.
- Hirshberg, D. A., Maleki, A., and Zubizarreta, J. R. (2021), “Minimax Linear Estimation of the Retargeted Mean,” .
- Hirshberg, D. A. and Wager, S. (2020), “Augmented Minimax Linear Estimation,” .
- Horwitz, L. I., Bernheim, S. M., Ross, J. S., Herrin, J., Grady, J., Krumholz, H. M., Drye, E. E., and Lin, Z. (2017), “Hospital characteristics associated with risk-standardized readmission rates,” *Medical Care*, 55, 528–534.
- Kallus, N. (2020), “Generalized Optimal Matching Methods for Causal Inference,” *Journal of Machine Learning Research*, 21, 1–54.
- Kang, J. D. Y. and Schafer, J. L. (2007), “Demystifying double robustness: a comparison of alternative strategies for estimating a population mean from incomplete data (with discussion),” *Statistical Science*, 22, 523–539.
- Kern, H. L., Stuart, E. A., Hill, J., and Green, D. P. (2016), “Assessing methods for generalizing experimental impact estimates to target populations,” *Journal of Research on Educational Effectiveness*, 9, 103–127.
- Kumar, S., Mohri, M., and Talwalkar, A. (2012), “Sampling methods for the Nyström method,” *The Journal of Machine Learning Research*, 13, 981–1006.
- Lawton, J. S., Tamis-Holland, J. E., Zwischenberger, B. A., et al. (2022), “2021 ACC/A-

- HA/SCAI Guideline for Coronary Artery Revascularization,” *Journal of the American College of Cardiology*, 79, e21–e129.
- Lehoucq, R. B., Sorensen, D. C., and Yang, C. (1998), *ARPACK users’ guide: solution of large-scale eigenvalue problems with implicitly restarted Arnoldi methods*, SIAM.
- Li, M., Bi, W., Kwok, J. T., and Lu, B.-L. (2014), “Large-scale Nyström kernel matrix approximation using randomized SVD,” *IEEE transactions on neural networks and learning systems*, 26, 152–164.
- Little, R. J. and Rubin, D. B. (2019), *Single imputation methods*, Wiley Online Library.
- Micchelli, C. A., Xu, Y., and Zhang, H. (2006), “Universal Kernels.” *Journal of Machine Learning Research*, 7, 2651–2667.
- Mohri, M. and Talwalkar, A. (2011), “Can matrix coherence be efficiently and accurately estimated?” in *Proceedings of the fourteenth international conference on artificial intelligence and statistics*, JMLR Workshop and Conference Proceedings, pp. 534–542.
- O’donoghue, B., Chu, E., Parikh, N., and Boyd, S. (2016), “Conic optimization via operator splitting and homogeneous self-dual embedding,” *Journal of Optimization Theory and Applications*, 169, 1042–1068.
- Pourkamali-Anaraki, F., Becker, S., and Wakin, M. (2018), “Randomized clustered nyström for large-scale kernel machines,” in *Proceedings of the AAAI Conference on Artificial Intelligence*, vol. 32.
- Robins, J. M. and Rotnitzky, A. (1995), “Semiparametric efficiency in multivariate regression models with missing data,” *Journal of the American Statistical Association*, 90, 122–129.
- Rosenbaum, P. R. and Rubin, D. B. (1983), “The central role of the propensity score in observational studies for causal effects,” *Biometrika*, 70, 41–55.

- Rubin, D. B. (1974), “Estimating causal effects of treatments in randomized and nonrandomized studies.” *Journal of Educational Psychology*, 66, 688.
- (2006), “The design versus the analysis of observational studies for causal effects: Parallels with the design of randomized trials,” *Statistics in Medicine*, 26, 20–36.
- Shah, B. R., Glickman, S. W., Liang, L., Gibler, W. B., Ohman, E. M., Pollack, C. V., Roe, M. T., and Peterson, E. D. (2007), “The impact of for-profit hospital status on the care and outcomes of patients with non-ST-segment elevation myocardial infarction: results from the CRUSADE Initiative,” *Journal of the American College of Cardiology*, 50, 1462–1468.
- Sloan, F. A., Trogon, J. G., Curtis, L. H., and Schulman, K. A. (2003), “Does the ownership of the admitting hospital make a difference? Outcomes and process of care of Medicare beneficiaries admitted with acute myocardial infarction,” *Medical Care*, 41, 1193–1205.
- Stellato, B., Banjac, G., Goulart, P., Bemporad, A., and Boyd, S. (2020), “OSQP: an operator splitting solver for quadratic programs,” *Mathematical Programming Computation*, 12, 637–672.
- Tran, D., Toulis, P., and Airolidi, E. M. (2015), “Stochastic gradient descent methods for estimation with large data sets,” *arXiv preprint arXiv:1509.06459*.
- Vu, T., Chunikhina, E., and Raich, R. (2021), “Perturbation expansions and error bounds for the truncated singular value decomposition,” *Linear Algebra and its Applications*, 627, 94–139.
- Wahba, G. (1990), *Spline models for observational data*, SIAM.
- Wang, S., Gittens, A., and Mahoney, M. W. (2019), “Scalable kernel K-means clustering with Nyström approximation: relative-error bounds,” *The Journal of Machine Learning Research*, 20, 431–479.

- Wang, Y. and Zubizarreta, J. R. (2020), “Minimal dispersion approximately balancing weights: asymptotic properties and practical considerations,” *Biometrika*, 107, 93–105.
- Wong, R. K. and Chan, K. C. G. (2018), “Kernel-based covariate functional balancing for observational studies,” *Biometrika*, 105, 199–213.
- Wood, S. N., Goude, Y., and Shaw, S. (2015), “Generalized additive models for large data sets,” *Journal of the Royal Statistical Society: Series C*, 64, 139–155.
- Xiong, S., Dai, B., Huling, J., and Qian, P. Z. (2016), “Orthogonalizing EM: A design-based least squares algorithm,” *Technometrics*, 58, 285–293.
- Zeng, Y. and Breheny, P. (2017), “The biglasso package: A memory-and computation-efficient solver for lasso model fitting with big data in R,” *arXiv preprint arXiv:1701.05936*.
- Zhao, Q. (2019), “Covariate balancing propensity score by tailored loss functions,” *Annals of Statistics*, 47, 965 – 993.
- Zhou, L., Pan, S., Wang, J., and Vasilakos, A. V. (2017), “Machine learning on big data: Opportunities and challenges,” *Neurocomputing*, 237, 350–361.
- Zubizarreta, J. R. (2015), “Stable weights that balance covariates for estimation with incomplete outcome data,” *Journal of the American Statistical Association*, 110, 910–922.

Supplementary Material for “Scalable kernel balancing weights in a nationwide observational study of hospital profit status and heart attack outcomes” by Kwangho Kim, Bijan A. Niknam, and José R. Zubizarreta

Appendix A. Proof of Theorem 1

We use three matrix norms for our result: for a matrix A with the (i, j) -entry a_{ij} , we define

$$\begin{aligned} \text{Frobenius Norm: } \|A\|_F &= \sqrt{\sum_{i,j} a_{ij}^2} = \sqrt{\sum_i \sigma_i^2(A)} \\ \text{Spectral Norm: } \|A\|_2 &= \max_{\|x\|_2=1} \|Ax\|_2 = \sigma_1(A) \\ \text{Trace Norm: } \|A\|_* &= \sum_i \sigma_i(A). \end{aligned}$$

Proof. Recall that from Section 3.1,

$$\begin{aligned} \widetilde{\mathbf{K}} &= CW^+C^\top, \\ \widetilde{\mathbf{K}}_l &= CW_l^{-1}C^\top, \\ (\widetilde{\mathbf{K}}_l)_s &= DD^\top \quad \text{where } D = CU_{W,l}\Lambda_{W,l}^{-1/2}\widetilde{V}_{R,s}. \end{aligned}$$

Let $w_t = \frac{1}{n_t}\mathbf{1}_{n_t}$. Then by the Cauchy–Schwarz and triangle inequalities, we have that

$$\begin{aligned} & \left| (\widehat{w}_c^\top U_c - w_t^\top U_t) \Lambda U^\top \alpha \right| \\ & \leq \left| (\widehat{w}_c^\top U_c - w_t^\top U_t) \Lambda U^\top \alpha - (\widehat{w}_c^\top D_c - w_t^\top D_t) D^\top \alpha + (\widehat{w}_c^\top D_c - w_t^\top D_t) D^\top \alpha \right| \\ & \leq \|\widehat{w}_c\|_2 \left\| U_c \Lambda U^\top - D_c D^\top \right\|_2 \|\alpha\|_2 + \|w_t\|_2 \left\| U_t \Lambda U^\top - D_t D^\top \right\|_2 \|\alpha\|_2 \\ & \quad + \left| (\widehat{w}_c^\top D_c - w_t^\top D_t) D^\top \alpha \right| \\ & \leq 2 \left\| \mathbf{K} - (\widetilde{\mathbf{K}}_l)_s \right\|_2 \|\alpha\|_2 + \left| (\widehat{w}_c^\top D_c - w_t^\top D_t) D^\top \alpha \right| \\ & \leq 2 \left\{ \left\| \mathbf{K} - (\widetilde{\mathbf{K}})_s \right\|_2 + \left\| (\widetilde{\mathbf{K}})_s - (\widetilde{\mathbf{K}}_l)_s \right\|_2 \right\} \|\alpha\|_2 + \left| (\widehat{w}_c^\top D_c - w_t^\top D_t) D^\top \alpha \right|. \end{aligned}$$

When $\|\widetilde{\mathbf{K}} - \widetilde{\mathbf{K}}_l\|_2 \leq \frac{\sigma_l - \sigma_{l+1}}{2}$, by Vu et al. (2021, Theorem 1), we have the following first-order approximation

$$\begin{aligned} \|(\widetilde{\mathbf{K}})_s - (\widetilde{\mathbf{K}}_l)_s\|_2 &\lesssim \|\widetilde{\mathbf{K}} - \widetilde{\mathbf{K}}_l\|_2 + \sum_{i=1}^l \sum_{j=l+1}^n \left(\frac{\sigma_j^2}{\sigma_i^2 - \sigma_j^2} + \frac{\sigma_i \sigma_j}{\sigma_i^2 - \sigma_j^2} \right) \|\widetilde{\mathbf{K}} - \widetilde{\mathbf{K}}_l\|_2 + \|\widetilde{\mathbf{K}} - \widetilde{\mathbf{K}}_l\|_F^2 \\ &\lesssim \|W^+ - W_l^{-1}\|_2 + \|W^+ - W_l^{-1}\|_F^2. \end{aligned}$$

Also, by Theorem 1 of Wang et al. (2019), we have

$$\begin{aligned}\|\mathbf{K} - (\widetilde{\mathbf{K}})_s\|_2 &\leq \|\mathbf{K} - (\widetilde{\mathbf{K}})_s\|_* \\ &\leq (1 + \epsilon) \|\mathbf{K} - \mathbf{K}_s\|_*\end{aligned}$$

with high probability at least 0.9.

For the last term in the last display, by the Cauchy–Schwarz inequality it follows that

$$\begin{aligned}\sup_{\alpha} \left| (\widehat{w}_c^\top D_c - w_t^\top D_t) D^\top \alpha \right| &\leq \left\| \widehat{w}_c^\top D_c - w_t^\top D_t \right\|_2 \sup_{\alpha} \left\| D^\top \alpha \right\|_2 \\ &\lesssim \left\| \widehat{w}_c^\top D_c - w_t^\top D_t \right\|_1 \\ &\lesssim \delta.\end{aligned}$$

Hence, provided that $\sup_{\alpha} \|\alpha\|_2 < \infty$, putting the two pieces together we have the desired probabilistic bound

$$\begin{aligned}&\sup_{\alpha} \left| (\widehat{w}_c^\top U_c - w_t^\top U_t) \Lambda U^\top \alpha \right| \\ &= (1 + \epsilon) \|\mathbf{K} - \mathbf{K}_s\|_* + O\left(\|W^+ - W_l^{-1}\|_2 + \|W^+ - W_l^{-1}\|_F^2 + \delta\right).\end{aligned}$$

□

Appendix B. More details on ADMM and OSQP

Convex QPs such as (4) are well-studied and various solution methods exist. Some commonly used solution methods include active-set, interior-point, and operator splitting methods. Active-set methods are the traditional algorithms for solving QPs. These algorithms explore the feasible region containing the solution by iteratively adding and dropping active constraints until the solution is found. Interior-point methods, the default algorithms used by many modern commercial solvers, solve unconstrained optimization problems for varying barrier functions until the optimum is achieved.

Typically, active-set methods outperform interior-point methods when the number of covariates or constraints is small, or when warm starts are used. Otherwise, interior-point methods generally outperform active-set methods in terms of scalability and speed. That said, in general the iteration costs of interior-point methods grow non-linearly with the dimensionality of the problem, rendering them impractical for very large-scale settings. Alternatively, operator splitting methods obtain an optimal solution using only first-order information about the cost function (i.e., the subgradients). They reduce the optimization problem to that of finding zeros of the sum of monotone operators. Here, we focus on a particular class of operator splitting methods known as the alternating direction method of multipliers (ADMM) (Boyd et al. 2011)) which has been shown to extend very well to large-scale convex optimization problems.

ADMM. The *Alternating direction method of multipliers* is likely the most commonly used operator splitting method due to its simplicity and ability to accommodate large problems. ADMM solves problems of the form

$$\begin{aligned} & \text{minimize} && g(\tilde{v}) + h(v) \\ & \text{subject to} && G\tilde{v} + Hv = q \end{aligned} \tag{16}$$

for two sets of variables \tilde{v} and v . Following Stellato et al. (2020), we introduce auxiliary variables \tilde{w} and \tilde{z} and write Problem (12) as

$$\begin{aligned} & \text{minimize} && \tilde{w}^\top \mathbb{1}_{n_c} \tilde{w} - \frac{1}{n_c} \tilde{w}^\top \mathbb{1}_{n_c} + \mathcal{I}_{Q_{w=z}}(\tilde{w}, \tilde{z}) + \mathcal{I}_{\mathcal{C}(\delta)}(z) \\ & \text{subject to} && \mathbb{1}_{1+2n_c+Kd}[\tilde{w}, \tilde{z}]^\top - \mathbb{1}_{1+2n_c+Kd}[w, z]^\top = 0, \end{aligned} \tag{17}$$

where \mathcal{I}_S is the indicator function for the set S . Problem (17) is in the ADMM form given by (16), where $g(\tilde{w}, \tilde{z}) = \tilde{w}^\top \mathbb{1}_{n_c} \tilde{w} - \frac{1}{n_c} \tilde{w}^\top \mathbb{1}_{n_c} + \mathcal{I}_{Q_{w=z}}(\tilde{w}, \tilde{z})$ and $h(w, z) = \mathcal{I}_{\mathcal{C}(\delta)}(z)$. Problem (17) can be solved via the following ADMM iterations

$$(w^{k+1}, \tilde{z}^{k+1}) \leftarrow \arg \min_{Q_{w=z}} w^\top \mathbb{1}_{n_c} w - \frac{1}{n_c} w^\top \mathbb{1}_{n_c} + \frac{\sigma}{2} \|x - w^k\|^2 + \frac{\rho}{2} \left\| z - z^k + \frac{y^k}{\rho} \right\|^2 \tag{18}$$

$$z^{k+1} \leftarrow \Pi_{\mathcal{C}(\delta)} \left(\tilde{z}^{k+1} + \frac{y^k}{\rho} \right) \tag{19}$$

$$y^{k+1} \leftarrow y^k + \rho (\tilde{z}^{k+1} - z^{k+1}) \tag{20}$$

Algorithm 2: OSQP for SBW

input : $Q, l(\delta), u(\delta)$
parameter: $\rho > 0, \sigma > 0, \alpha \in (0, 2)$
1 Initialize w^0, y^0, z^0, ν^0 and set $k = 0$
2 **repeat**
3 $(\tilde{w}^{k+1}, \nu^{k+1}) \leftarrow \text{solve } \begin{bmatrix} -(1 + \sigma)\mathbb{1}_{n_c} & -Q^\top \\ -Q & \rho^{-1}\mathbb{1} \end{bmatrix} \begin{bmatrix} \tilde{w}^{k+1} \\ \nu^{k+1} \end{bmatrix} = - \begin{bmatrix} \sigma w^k - 1/n_c \mathbb{1}_{n_c} \\ z^k - \rho^{-1} y^k \end{bmatrix};$
4 $\tilde{z}^{k+1} \leftarrow z^k + \rho^{-1}(\nu^{k+1} - y^k)$
5 $w^{k+1} \leftarrow \alpha \tilde{w}^{k+1} + (1 - \alpha)w^k$
6 $z^{k+1} \leftarrow \Pi_{\mathcal{C}(\delta)}(\alpha \tilde{z}^{k+1} + (1 - \alpha)z^k + \rho^{-1}y^k)$
7 $y^{k+1} \leftarrow y^k + \rho(\alpha \tilde{z}^{k+1} + (1 - \alpha)z^k - z^{k+1})$
8 $k \leftarrow k + 1$
9 **until** *termination criterion satisfied*;

where y is a dual covariate, $\sigma, \rho > 0$ are step-size parameters, and $\Pi_{\mathcal{C}(\delta)}$ denotes the Euclidean projection onto $\mathcal{C}(\delta)$ (see Boyd et al. 2011 for details).

ADMM blends the advantages of dual decomposition and the method of multipliers (or the augmented Lagrangian method). First, as a method of multipliers, ADMM exhibits excellent convergence properties. In fact, Problem (16) does not require any assumptions for convergence beyond convexity of g and h and that its augmented Lagrangian has a saddle point, an advantage not shared by other operator splitting methods. Second, as described by the steps in equations (18) and (19), in ADMM w^k and z^k are updated sequentially or alternately, where each step is typically far less expensive than the original minimization problem jointly over (w, z) . Indeed, the inner QP (18) is an equality-constrained problem which can be reduced to solving a linear system, and (19) is simply a box projection. This decomposability therefore substantially reduces the computational burden required for execution, and allows ADMM to find solutions much faster than conventional methods.

Despite these appealing features, ADMM has some limitations. One potential limitation is its inability to detect infeasibility. Moreover, it loses its speed advantage when aiming to find high-accuracy solutions, and its convergence rates also highly depend on the parameter selection and the data setting. Despite these challenges, significant progress has recently been made in adapting ADMM to very large-scale convex optimization problems. O’donoghue et al. (2016) and Fougner and Boyd (2018) proposed the splitting-based conic solver (SCS) and proximal operator graph-form solver (POGS), respectively. Based on their own parameter selection heuristics and data preconditioning, they showed that both SCS and POGS scale well to extremely large problems, with SCS also able to detect infeasibility. More recently, Stellato et al. (2020) developed the operator splitting solver for quadratic programs (OSQP), a state-of-the-art ADMM-based solver particularly tailored to general QPs. OSQP is the first generic QP solver that addresses all three challenges of detecting infeasibility, finding high-accuracy solutions, and adapting to different data settings.

OSQP for SBW. For convenience, the OSQP algorithm for SBW is presented in Algorithm

2 separately from Figure 1. Steps 3 and 4 correspond to the reduced Karush-Kuhn-Tucker (KKT) system for the inner QP (18), and Steps 6 and 7 correspond to (19) and (20), respectively. In Steps 5, 6, and 7, the relaxation method is used for the w -, z -, and y -updates with the relaxation parameter α . The termination criterion is satisfied when both the primal and dual residuals are smaller than some prespecified tolerance, or if infeasibility is detected with some prespecified level of accuracy. Although the method of choosing the optimal parameters (ρ, σ, α) may vary, Stellato et al. (2020) provides guidance for doing so with OSQP. The parameter σ behaves like a regularization term and can be as small as possible, so long as it ensures that a unique solution of the linear system in Step 3 of Algorithm 2 exists. Also, through extensive empirical research, it has been shown that setting the relaxation parameter α in the range $[1.5, 1.8]$ generally improves the convergence rate. To set the step size ρ , OSQP adopts heuristics that assign higher values for active constraints and lower values for inactive constraints. Furthermore, to ensure fast convergence over a wide range of problems, the algorithm uses the ratio between the primal and dual residuals to adaptively update ρ from one iteration to the next. Stellato et al. (2020) showed that the proposed parameter selection heuristics in OSQP exhibit solid improvements in terms of convergence and stability.

We remark that POGS and SCS are alternative ADMM-based methods that could be applied; however, these approaches require reformulation of our QP, which introduces many extra coefficients into the optimization procedure and therefore may not be computationally efficient (Stellato et al. 2020).

Appendix C. RMSE under strong overlap

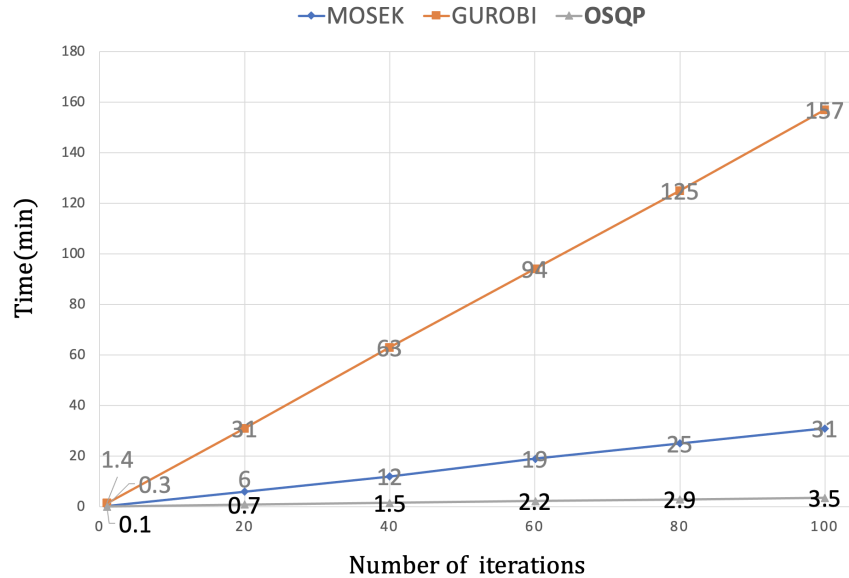
Results for under strong overlap are presented in Web Table 7.

Table 7: RMSE under weak overlap

Method		X correctly specified (X)					X transformed (X^*)					
		n	2k	5k	10k	100k	1M	2k	5k	10k	100k	1M
$\hat{\psi}_{\text{mod}}$	glm		1.13	0.72	0.48	0.40	0.40	1.31	0.80	0.56	0.41	0.40
	sgdglm		1.13	0.72	0.48	0.40	0.40	1.31	0.80	0.56	0.41	0.40
	glmnet		1.10	0.87	0.58	0.17	0.07	1.30	1.23	0.51	0.21	0.13
	biglasso		1.25	0.82	0.55	0.16	0.08	1.30	1.02	0.50	0.21	0.12
	oem		1.23	0.82	0.58	0.17	0.08	1.33	1.49	0.71	0.22	0.13
	admm.lasso		1.78	0.87	0.58	0.22	0.14	2.23	1.12	0.56	0.27	0.16
	ranger		1.22	0.86	0.66	0.22	0.09	1.27	0.85	0.52	0.20	0.07
	kernel.ridge		1.18	0.84	0.67	0.29	M	1.53	0.91	0.67	0.32	M
	bam		2.47	0.67	0.46	0.41	0.40	3.37	1.95	1.25	1.19	1.18
	$\hat{\psi}_{\text{bal}}$	quadprog		0.07	0.04	0.03	F	F	0.41	0.24	0.18	F
qpoases			0.07	0.05	F	F	F	0.41	0.28	F	F	F
gurobi			0.05	0.03	0.02	0.01	0.01	0.38	0.21	0.19	0.09	0.03
Rmosek			0.05	0.03	0.02	0.01	0.01	0.38	0.21	0.19	0.09	0.03
osqp			0.05	0.03	0.02	0.01	0.01	0.39	0.21	0.19	0.10	0.03
pogs			0.7	0.04	0.03	M	M	0.40	0.25	0.25	M	M
scs			0.11	0.10	0.09	0.05	0.02	0.39	0.25	0.20	0.13	0.10

Appendix D. Time reduction via factorization caching and warm starting

Figure 2: Average cumulative CPU time over multiple iterations of SBW calls



Since the vectors l, u are the only parameters that vary in δ in Algorithm 2, we can speed up repeated OSQP calls via factorization caching and warm starting. Specifically, although the tuning procedure requires a number of iterations, because the coefficient matrix in the relevant linear system is fixed across iterations and does not depend on δ , factorization caching can be used, storing the factorization from the first iteration for use in subsequent ones. Also, because small changes in δ do not substantially affect weighting solutions, warm starting can be used for added efficiency. To illustrate this computational gain, we solve a sequence of OSQP-based SBW problems using 100 values of δ equally spaced between 0.001 and 0.1 on the same data, and compare its computing time against two popular commercial solvers `gurobi` and `Rmosek` (with the default setting of interior-point methods). Data are generated by the same simulation setup used in Section 4 under weak overlap. We measure the cumulative time for each solver at $m = 1, 20, 40, 60, 80, 100$ problem instances across different values of δ . We repeat the simulation 100 times and present their average values in Web Figure 2.

For `gurobi` and `Rmosek`, the cumulative time increases linearly with the number of iterations as would be expected; i.e., m iterations took roughly m times as long as a single execution. However, m iterations of the OSQP algorithm took much less time than $m \times$ (the execution time for a single run); in fact, it is on average 2.4 times faster. This 2.4-fold time improvement demonstrates the benefits of factorization caching and warm starting via OSQP when implementing SBW.

Appendix E. Complete case study balance table before and after stable kernel balancing

Covariate	For-Profit	Unweighted Controls	Weighted Controls	TASMD Before	TASMD After
Age at Admission	79.043	79.322	79.035	0.034	0.001
Age 66-74	0.369	0.360	0.367	0.019	0.005
Age 75-84	0.371	0.365	0.371	0.012	0.002
Age 85+	0.260	0.275	0.262	0.034	0.004
Admission Year	2014.771	2014.668	2014.778	0.039	0.002
Admission 2010	0.029	0.030	0.029	0.008	0.000
Admission 2011	0.110	0.118	0.109	0.027	0.002
Admission 2012	0.112	0.117	0.112	0.016	0.001
Admission 2013	0.107	0.112	0.108	0.016	0.001
Admission 2014	0.109	0.108	0.108	0.004	0.004
Admission 2015	0.111	0.108	0.111	0.010	0.000
Admission 2016	0.113	0.110	0.113	0.009	0.001
Admission 2017	0.114	0.108	0.116	0.019	0.003
Admission 2018	0.099	0.098	0.100	0.003	0.003
Admission 2019	0.094	0.089	0.094	0.018	0.002
Sex (female)	0.478	0.477	0.477	0.003	0.002
Non-Hispanic White	0.790	0.842	0.794	0.128	0.008
Black	0.083	0.078	0.082	0.019	0.004
Hispanic	0.086	0.044	0.085	0.148	0.003
Asian/Pacific Islander	0.025	0.019	0.025	0.039	0.001
Native American	0.005	0.005	0.004	0.007	0.019
Other Race	0.011	0.012	0.011	0.013	0.001
Emergent Admission	0.837	0.838	0.836	0.002	0.003
Anterior ST-elevation MI 1	0.069	0.077	0.069	0.032	0.002
Other ST-elevation MI	0.149	0.156	0.150	0.018	0.002
History of PCI	0.150	0.159	0.152	0.024	0.004
History of CABG	0.119	0.119	0.119	0.001	0.001
Hx Sepsis	0.015	0.014	0.015	0.005	0.001
Hx Infection	0.002	0.002	0.002	0.001	0.001
Hx Metastatic Cancer	0.011	0.013	0.011	0.024	0.001
Hx Metastatic or Severe Cancer	0.022	0.025	0.022	0.024	0.001
Hx Lung or Severe Cancer	0.014	0.016	0.014	0.015	0.001
Hx Non-metastatic Cancer	0.029	0.034	0.030	0.027	0.003
Hx Cancer, Other	0.003	0.004	0.002	0.009	0.015
Hx Diabetes	0.376	0.371	0.375	0.010	0.002
Hx Diabetes w/ Complications	0.129	0.134	0.130	0.015	0.002
Hx Diabetes w/o Complications	0.083	0.072	0.083	0.040	0.002
Hx Malnutrition	0.042	0.036	0.041	0.031	0.005
Hx Morbid Obesity	0.677	0.695	0.679	0.037	0.003

Hx Liver Disease	0.016	0.017	0.016	0.006	0.000
Hx Dementia	0.139	0.131	0.138	0.022	0.002
Hx Substance Use	0.117	0.113	0.117	0.012	0.000
Hx Major Psychiatric Disorder	0.018	0.017	0.019	0.010	0.001
Hx Cardio-respiratory Failure or Shock	0.160	0.159	0.159	0.002	0.003
Hx Heart Failure	0.435	0.438	0.436	0.006	0.002
Hx AMI	0.006	0.007	0.006	0.007	0.001
Hx Unstable Angina	0.065	0.062	0.065	0.011	0.000
Hx Valvular Disease	0.156	0.191	0.159	0.095	0.006
Hx Hypertensive Heart Disease	0.021	0.016	0.021	0.035	0.000
Hx Hypertension	0.476	0.477	0.476	0.002	0.000
Hx Arrhythmia, Specified	0.285	0.289	0.286	0.008	0.003
Hx Arrhythmia, Other	0.129	0.152	0.130	0.070	0.005
Hx Stroke	0.007	0.007	0.005	0.003	0.022
Hx Cerebrovascular Disease	0.040	0.045	0.039	0.026	0.002
Hx Precerebral Occlusion	0.032	0.036	0.032	0.025	0.000
Hx Peripheral Vascular Disease	0.058	0.062	0.059	0.014	0.001
Hx Lung Fibrosis	0.017	0.019	0.017	0.019	0.001
Hx Asthma	0.028	0.033	0.029	0.027	0.002
Hx COPD	0.215	0.202	0.213	0.032	0.004
Hx Pneumonia	0.100	0.088	0.099	0.039	0.002
Hx Pneumothorax	0.019	0.018	0.019	0.007	0.001
Hx Other Respiratory Disease	0.064	0.070	0.065	0.023	0.003
Hx Eye, Other	0.010	0.012	0.011	0.015	0.003
Hx Renal Failure	0.364	0.359	0.364	0.009	0.000
Hx UTI	0.089	0.078	0.088	0.039	0.004
Hx Male Genital Disorder	0.087	0.092	0.088	0.018	0.004
Hx Skin Ulcer	0.022	0.024	0.022	0.016	0.002
Hx Skin Disease, Other	0.010	0.013	0.010	0.027	0.000
Hx Iatrogenic Complication	0.035	0.037	0.035	0.010	0.001
Hx Trauma	0.023	0.024	0.024	0.006	0.003
<i>County Hospital Characteristics</i>					
Urban Hospital	0.881	0.877	0.883	0.010	0.006
Large Size (501+ Beds)	0.052	0.077	0.052	0.338	0.007
Medium Size (251-100 Beds)	0.153	0.194	0.154	0.305	0.006
Small Size (Under 251 Beds)	0.795	0.729	0.793	0.442	0.009
Resident-to-Bed Ratio	0.021	0.034	0.021	0.336	0.002
Major Teaching (RTB \geq 0.25)	0.026	0.039	0.026	0.195	0.006
Minor Teaching ($0 \leq$ RTB \leq 0.25)	0.098	0.146	0.098	0.390	0.001
Nonteaching (RTB=0)	0.876	0.815	0.876	0.407	0.001
Nurse-to-Bed Ratio	0.971	1.063	0.977	0.120	0.008
High NTB (NTB \geq 1.0)	0.376	0.421	0.377	0.214	0.002
Moderate NTB ($0.9 \leq$ NTB $<$ 1.0)	0.053	0.052	0.053	0.009	0.005
Low NTB (NTB $<$ 0.9)	0.571	0.527	0.571	0.208	0.000

Cardiac Technology Index	0.921	1.022	0.921	0.263	0.000
Cardiac Surgery Provided	0.246	0.280	0.246	0.234	0.004
Coronary Care Unit	0.411	0.480	0.412	0.330	0.005
Cardiac Catheterization Lab	0.265	0.262	0.263	0.012	0.009
All Three Cardiac Services Available	0.140	0.154	0.137	0.112	0.022
